To: J Neurosci 2018-10-27.docx

Glutamate uptake and release at single adult corticostriatal synapses of normal and Huntington mice

Anton Dvorzhak[a], Nordine Helassa[b,c], Katalin Török[b], Dietmar Schmitz[a], Rosemarie Grantyn[a*]

[a] Cluster of Excellence Neurocure, Charité -University Medicine Berlin, Germany, [b]Molecular and Clinical Sciences Research Institute, St. Georges's, University of London, United Kingdom, [c]Department of Cellular and Molecular Physiology, Institute of Translational Medicine, University of Liverpool, United Kingdom

[*] Author for correspondence at the following address:
Prof. Rosemarie Grantyn
Synaptic Dysfunction Group
Cluster of Excellence Neurocure, Charité -University Medicine Berlin
Robert-Koch-Platz 4
D-10115 Berlin, Germany
Email: rosemarie.grantyn@charite.de

27 pages, 7 figures, 3 tables, link to video
Number of words: Abstract – 250, Introduction – 628, Discussion – 1454

No conflict of interest to declare

ACKNOWLEDGEMENT

We thank V. Beaumont, H. Kettenmann and S. Hirschberg for helpful discussions. D. Betances, A. Schönherr and J. Rösner provided skilled technical assistance. The work in the Grantyn lab was supported by CHDI (A-12467), the German Research Council (Exc 257/1) and intramural Charité Research Funds.

ABSTRACT

Changes in the balance between synaptic glutamate (Glu) release and uptake may stimulate synaptic reorganization and even synapse loss. The search for the primary cause of a potential mismatch between uptake and release should be easier if both parameters are assessed independently and at a single synapse level. This has now become possible due to a new imaging assay with the genetically encoded ultrafast Glu sensor $iGlu_u$. We report results obtained from individual corticostriatal synapses in acute slices prepared from mice aged >1 year. Contrasting patterns of short-term plasticity and a size criterion identified 2 classes of terminals, presumably corresponding to the previously defined IT and PT synapses. The latter exhibited a higher degree of frequency potentiation/residual Glu accumulation and were selected for investigation in the Q175 mouse model of Huntington's disease (HD). It was found that in HD the time constant of perisynaptic [Glu] decay (TauD, as indicator of uptake) and the maximal [Glu] next to the presynaptic terminal (as indicator of release) were prolonged and reduced, respectively. According to these criteria, about 30% of P terminals tested in Q175 heterozygotes (HET) were diagnosed as sick. HD but not WT synapses exhibited a positive correlation between TauD and the peak amplitude of $iGlu_u$. Treatment of WT preparations with the Glu uptake blocker TFB-TBOA (100 nM) mimicked the TauD changes in homozygotes (HOM). The NMDAR-mediated unitary EPSCs elicited by optical activation of single ChR-expressing corticostriatal axons were prolonged, and less EAAT2 immunoreactivity was found in the environment of corticostriatal terminals.

SIGNIFICANCE STATEMENT

Alterations in astrocytic Glu uptake can play a role in synaptic plasticity and neurodegeneration. Until now, sensitivity of synaptic responses to pharmacological transport block and the resulting activation of NMDA receptors were regarded as reliable evidence for a mismatch between synaptic uptake and release. But the latter parameters are interdependent. Using a new genetically encoded sensor to monitor [Glu] at individual corticostriatal synapses we are now able to quantify the time constant of perisynaptic [Glu] decay (as indicator of uptake) and the maximal [Glu] next to the active zone (as indicator of Glu release). The results provide a positive answer to the hitherto unresolved question whether neurodegeneration (e.g.

Huntington's disease) associates with a glutamate uptake deficit at tripartite excitatory synapses.

INTRODUCTION

A low level of steady state glutamate concentration [Glu] is an important prerequisite for high spatial and temporal discrimination of afferent signals. Electrogenic transport of Glu from the environment of active synaptic terminals into astroglial cells secures resting [Glu] levels below 100 nm (Bergles et al., 1999; Marcaggi and Attwell, 2004; Tzingounis and Wadiche, 2007; Nedergaard and Verkhratsky, 2012; Papouin et al., 2017; Rose et al., 2018). Compared to other synaptically enriched proteins, including the AMPA receptors, excitatory amino acid transport proteins (EAAT1 and EAAT2, GLAST and GLT1 in rodents) are very abundant (Lehre and Danbolt, 1998; Marcaggi and Attwell, 2004; Cahoy et al., 2008) forming clusters on the perisynaptic astroglial processes (PAPs) next to the sites of transmitter release (Lehre and Danbolt, 1998; Melone et al., 2011). However, the proximity between the sites of synaptic Glu release and astrocytic uptake could vary according to the type of synapse or the functional state of the involved cells (Octeau et al., 2018).

Insufficient expression/activity of EAAT2 is considered among the mechanisms promoting excitotoxic damage and neurodegeneration (Pekny et al., 2016; Verkhratsky et al., 2016). As for HD, there is full agreement that transcription of the EAAT2 encoding gene *SLC1A2* and tissue uptake of radio-labelled EAAT2 substrates are reduced in comparison with healthy controls (Lievens et al., 2001; Behrens et al., 2002; Shin et al., 2005; Miller et al., 2008; Bradford et al., 2009; Faideau et al., 2010; Huang et al., 2010; Menalled et al., 2012; Grewer et al., 2014; Meunier et al., 2016). Records from striatal astrocytes (Dvorzhak et al., 2016) suggested a 20-30% decrease of the glutamate uptake activity in two mouse models of HD, R6/2 and Q175. Yet some caution is needed as it has remained unclear whether or not the well-documented reduction of astrocytic Glu transport is to be regarded as a primary cause of synapse dysfunction or loss, or merely represents an epiphenomenon reflecting glial adjustment to the massive pruning of glutamatergic terminals for other yet unknown reasons (Deng et al., 2013; Rothe et al., 2015).

As synapse degeneration is likely to progress in a rather asynchronous manner resulting in a co-existence of sick and more or less healthy terminals, a satisfying answer to the question of functional adequacy of astrocytic glutamate uptake in HD can only be obtained at the single synapse level and under consideration of the individual uptake/release relationships (Barbour, 2001; Nahir and Jahr, 2013; Jensen et al., 2017; Reynolds et al., 2018).

The striatum as the most affected brain structure in HD (Khakh et al., 2017) is well suited for selective activation of glutamatergic synapses as it lacks intrinsic glutamatergic neurons. Glutamatergic afferents originate in the medial thalamus and the cerebral cortex (see (Reiner and Deng, 2018) for more). Corticostriatal connections are formed by at least two distinct populations of pyramidal neurons, localized in layers 2/3 and 5. The axons originating in layer 2/3 establish bilateral intra-telencephalic (IT) connections, while layer 5 axons enter the pyramidal tract (PT) and lack telencephalic collaterals to the contralateral side. Elegant electrophysiology (Kincaid et al., 1998) and electron microscopy studies (Reiner et al., 2010) discovered a number of differences between PT and IT afferents and their synaptic varicosities. In view of this diversity one could expect some type-dependent differences in the release characteristics and, accordingly, differential sensitivity to factors that may cause an uptake/release imbalance.

Here we report the results of the first single synapse experiments in striatal slices of adult mice performed with the ultrafast Glu sensor iGlu$_u$ (Helassa et al., 2018). We have addressed three main questions: 1) How does activation frequency affect the Glu release and uptake at corticostriatal terminals? 2) Does HD produce an uptake/release mismatch? 3) If so, would this mismatch be based on uptake insufficiency rather than excessive release?

MATERIALS AND METHODS

Animals. The work described here has been carried out in accordance with the EU Directive *2010/63/EU* for animal experiments and was registered at the Berlin Office of Health Protection and Technical Safety (G0233/14 and G0218/17). Z-Q175-KI mice were obtained from CHDI ("Cure Huntington's Disease Initiative", see stock #

027410 of the Jackson Laboratory). The number of CAG repeats ranged from 122 to 193. The recordings were performed at an age of 51 to 76 weeks.

Plasmids. pAAV-CaMKIIa-ChR2(H134R)-EYFP and pAAV-CaMKIIa-hChR2(E123T/T159C)-EYFP (Addgene #26969 and #35511) were gifts from Karl Deisseroth. To create pAAV-CaMKIIa-iGlu$_u$ (Addgene #75443), the iGlu$_u$ gene was amplified by PCR from pCI-syn-iGlu$_u$ (Addgene #106122) using Phusion polymerase (forward 5'-CATCAGGATCCATGGAGACAGACACACTCC-3', reverse 5'-GTATGGAATTCCTAACGTGGCTTCTTCTGCC-3') and cloned into pAAV-CaMKIIa-hChR2(H134R)-EYFP by restriction-ligation using BamHI/EcoRI restriction enzymes (NEB) and T4 DNA ligase (NEB). AAV9-CaMKIIa.iGlu$_u$.WPRE-hGH and AAV9-CaMKIIa.hChR2(E123T/T159C)-EYFP.hGH were packaged at University of Pennsylvania Vector Core (Penn Vector Core).

Drugs and antibodies. All the substances were obtained from Sigma Aldrich, except TTX (Abcam), CEF and TFB-TBOA (both Tocris). The primary antibodies included those to vGluT1 (1:1000, guinea pig, Synaptic Systems #135304) and EAAT2 (1:2000, rabbit, Abcam #ab41621). Secondary antibodies against guinea pig and rabbit, were conjugated to Alexa 488 or 555 and obtained from Life Technologies (#A-11073, #A-21429, respectively).

Injections and brain slice preparation. The animals were anesthetized by intraperitoneal injection of a mixture containing 87.5 mg/kg ketamine and 12.5 mg/kg xylasine before receiving 4 intracortical injections of AAV9-CamKII.iGlu$_u$.WPRE-hGH ($7.34*10^{13}$gcC/ml - 0.3 µl) or 1 intracortical injection of AAV9-CaMKIIa.hChR2(E123T/T159C)-EYFP.hGH ($6.28*10^{12}$ gc/ml - 1 µl) at the following coordinates with respect to bregma (mm): anterior 1.5, lateral 1.56, 1.8, 2.04, 2.28 and ventral 1.7. About 3 weeks (ChR2) or 6 weeks (iGlu$_u$) later the animals were anesthetized with isoflurane, transcardially perfused with cooled aerated saline containing (in mM): N-methylglucamine chloride (NMDG) 92, KCl 2.5, NaH_2PO_4 1.25, $NaHCO_3$ 25, glucose 20, $CaCl_2$ 0.5, $MgCl_2$ 10, sodium pyruvate 3, and sodium ascorbate 5 (pH 7.35, 303 mosmol/l). After decapitation and removals of the brains, parasagittal (10 deg off) sections (300 µm) containing the striatum were prepared as

previously described (Dvorzhak et al., 2016). The slices were kept in artificial cerebrospinal fluid (ACSF) containing (in mM): NaCl 125, KCl 3, NaH_2PO_4 1.25, $NaHCO_3$ 25, $CaCl_2$ 2, $MgCl_2$ 1, glucose 10 (pH 7.3, 303 mosmol/l), supplemented with (in mM): sodium pyruvate 0.5, sodium ascorbate 2.8 and glutathione 0.005. These perfusion and recovery solutions preserved the astrocytes better than physiological ACSF, sucrose- or choline-containing solutions, the criteria being resting membrane potential at break-in (WT: <=-85 mV). Ten Q175 HOM were also injected with CEF (5 consecutive days before testing, 200 mg/kg i.p.) or the respective control solution (physiological saline).

Quantification of perisynaptic [Glu] elevations with iGlu$_u$. The biophysical characteristics of the new ultrafast Glu sensor (iGlu$_u$) were already described (Helassa et al., 2018). Briefly, at 20 ^{o}C the responses of transduced HEK293T cells to saturating Glu concentration (10 mM) decayed with a time constant of 2.1 ms. For the imaging of synaptically released Glu, slices were submerged into a perfusion chamber with a constant flow of oxygenated ACSF at a rate of 1-2 ml/min. Temperature during the recordings was maintained at 26 - 27 °C. In non-stimulated acute slices from >1 year old mice corticostriatal varicosities were visualized in the dorsal striatum using a Zeiss W Plan-Apochromat 63x /NA 1.0 water immersion objective and brief (180 ms) discontinuous exposure to a 473 nm laser beam focused to a circular area of ~4.5 µm in diameter centered to a presynaptic varicosity. The distance to the nearest other fluorescent varicosity was typically 3 to 5 µm. The size of non-stimulated boutons was derived from the area of supra-threshold pixels, the threshold being defined as mean ROI intensity + 3 SD. For evaluation of evoked responses, the iGlu$_u$ fluorescence was acquired at a frequency of 2.5 kHz from a rectangular ROI of 4 µm x 4 µm (20 x 20 pixels, binning 2) using a sCMOS camera (Andor Zyla4.2 plus) attached to a Zeiss wide field microscope (AxioObserver). In-house written software routines controlled the laser, camera and electrical stimulation of the axon/bouton. Each pixel of the ROI was evaluated separately for the construction of time- and space-dependent [Glu] profiles after release. The iGlu$_u$ intensity values were expressed as supra-threshold pixel fluorescence ΔF in % of the mean baseline fluorescence derived from the data points acquired during a 50 ms period prior to stimulation.

For the description of the stimulus-induced changes of $iGlu_u$ we defined the following parameters. The term "p*eak amplitude*" or "m*ean ΔF/F at peak*" refers to the time-dependent changes ("transients") of mean ΔF/F values, as calculated from all supra-threshold pixels (see Fig. 1E for a specimen). The term "*maximal amplitude*" (see Fig. 5A-C) refers to the time-dependent changes ("transients") of the pixel with the highest elevation of $iGlu_u$ fluorescence after single pulse activation. Typically this would be a pixel in close proximity with the bouton borders delineated at rest. Accordingly, the TauD values either refer to the decay from peak or maximal amplitudes. If not mentioned otherwise, TauD is obtained by fitting a monoexponential function to the decay of individual evoked transients. "*Residual ΔF/F*" is derived from fitting a double exponential function to the decay of mean supra-threshold pixel values after the last stimulus. It roughly corresponds to the ΔF/F value at the intercept between the fast and slow phase of $iGlu_u$ decay (see Fig. 2*H*). "*Integral ΔF/F*" is the sum of all ΔF/F values during a period of 70 ms starting with the first stimulus (see Fig. 2*I*). The spatial extension of the $iGlu_u$ signal ("*Spread*") is defined as the diameter of the area of all suprathreshold pixels combined to form virtual circle.

Single axon/bouton activation. To induce the Glu release from individual synaptic boutons under physiological conditions, a depolarizing current pulse was applied through an ACSF-filled glass pipette (tip diameter <1 µM, resistance 10 MOhm) placed next to an axon in close proximity with a fluorescent varicosity. Responses were elicited at minimal intensity at a repetition frequency of 0.1 Hz. They disappeared when the pipette was moved by as little as 5 pixel diameters (1 µm). Single bouton recording of $iGlu_u$ in the presence of TTX was performed in elevated (5 mM) $[Ca^{2+}]_{ec}$ using a biphasic stimulation. For more details on single bouton activation and recording of unitary EPSCs see (Kirischuk et al., 1999; Kirischuk et al., 2002) and (Dvorzhak et al., 2013a).

Patch-clamp recording of unitary EPSCs (uEPSCs). uEPSCs were recorded in the presence of bicuculline methiodide (BMI) as previously described (Dvorzhak et al., 2013b). Briefly, the intra-pipette solution contained (in mM): cesium methane sulfonate 100, CsCl 50, NaCl 5, $CaCl_2$ 0.5, EGTA 2.5, Hepes 25, MgATP 2, GTP 0.3

(pH 7.2). uEPSC were induced via optical activation of APs in hChR2(E123T/T159C)-EYFP expressing corticostriatal axons. Using the point illumination system UGA-42 of Rapp OptoElectronic, the duration and size of the laser pulse was adjusted to activate a synaptic response with distinct threshold. Stimulation was accepted as minimal if the following criteria were satisfied: (i) uEPSC latency remained stable (fluctuations <20% of means, (ii) lowering stimulus duration by 20% resulted in a complete failure of uEPSCs, (iii) an increase in stimulus duration by 20% neither changed mean amplitude nor shape of uEPSCs. To elicit AMPAR- and NMDAR-mediated components of uEPSCs, records were performed at holding potentials of −70 mV and +50 mV, respectively.

Synaptic EAAT2 immunofluorescence. Using deep isoflurane anesthesia, mice were transcardially perfused with ice-cold phosphate-buffered saline (PBS) followed by a solution of 4% (w/v) paraformaldehyde in PBS. Sagittal sections (30 µm) were prepared as previously described (Rothe et al., 2015). Freely floating sections were double-stained with guinea pig anti-vGluT1 (1:1000) and rabbit anti EAAT2 (1:2000), followed by respective secondary antibodies at a concentration of 1:800. Images were acquired using a Zeiss 100x oil immersion objective (NA1.3). ROIs of 30 x 30 pixels (pixel size 0.074 µm) were centred to a single vGluT1 spot and the supra-threshold (Th = mean + 2.5 SD) EAAT2-positive pixels were determined for estimation of the mean the immunofluorescence (IF) intensity and area of the EAAT2+ spots. Evaluation was performed using Autoquant X3 (MediaCybernetics) for deconvolution of the vGluT1 images. The respective EAAT2 images were evaluated based on the original images using the Nemo 1.43 software routine of C. Henneberger. The sections from 4 WT and 4 Q175 HOM were stained together, and all images were acquired with the same camera settings (Spot Insight, Diagnostic Instruments).

Statistics. Data is presented as means ± s.e.m. and was analyzed by paired and unpaired t-test or the nonparametric Mann-Whitney test, one-way or two-way ANOVA or the respective non-parametric Kruskal-Wallis test with posthoc comparison of individual means, as indicated. P values of <0.05 was considered statistically significant. Significance levels were marked by asterisks, where * corresponds to

P<0.05, ** - P<0.01 and *** - P<0.001. The numbers indicate animals, cells or presynaptic terminals, as indicated in the figure legends or tables. HD-related differences are described in % of WT levels, ∆%WT (Tabs. 2, 3).

RESULTS

Evaluation of action potential-(AP-)mediated perisynaptic corticostriatal Glu transients using the new ultrafast sensor iGlu$_u$ in acute slices from adult mice

Placement of stimulating electrodes in the vicinity of corticostriatal terminals at rest was carried out under visual guidance (Fig. 1*A*). Bouton size was defined on the basis of resting fluorescence in the region of interest, ROI (Fig. 1, area boxed in blue). The deduced virtual diameter exhibited a bimodal distribution (Fig. 1*C*). Varicosities with a diameter <=0.57 µm were defined as “Small” and, for the sake of brevity, tentatively referred to as IT type. Accordingly, varicosities with d >=0.63 µm were classified as “Large” or PT type.

After electrical stimulation of a fluorescent corticostriatal axon in the dorsal striatum iGlu$_u$ intensity increased in the pixels adjacent to the area defined as resting terminal (Fig. 1*D*). Mean supra-threshold pixel intensity ∆F/F was plotted against time (Fig. 1*E*, middle trace), and a monoexponential function was fitted to the stimulus-induced iGlu$_u$ transient ∆F/F to determine TauD. In the case of single pulse activation, there was no significant correlation between TauD and bouton diameter (not illustrated).

The focus of the current experiments was placed on the time course of the iGlu$_u$ signals. The position of the sensor and its low affinity for Glu naturally set limits to the detection of [Glu] elevations at larger distance from the site of vesicle exocytosis. Nevertheless, we also expected some preliminary information on the spatial characteristics of the iGlu$_u$ signal. Therefore, a virtual diameter (“Spread”) was deduced from the projection of the supra-threshold iGlu$_u$ signal to the focal plane and plotted against time (Fig. 1*E*, lower trace). Under condition of single pulse activation “Spread” exhibited a significant positive correlation with TauD (Fig. 1*F*), but the mean values of maximal amplitude, peak amplitude, TauD and Spread were not different between the two types of terminals after single pulse activation (Tab. 1, Fig. 1*G*).

The differences between I- and P-type terminals became more obvious with repetitive stimulation. Activation with stimulus pairs at an interval of 50 ms revealed differences in the paired pulse ratios (PPR) of peak amplitudes resulting in a positive correlation between PPR and bouton diameter (Fig. 1H). This finding validated our size criterion for terminal separation and provided a first hint that IT and PT terminals may generate a differential load for Glu clearance when repeatedly activated.

Frequency-dependent potentiation of Glu release at PT but not IT corticostriatal terminals

As we aimed at exploring the limits of Glu release under conditions resembling the cortical activity during movement initiation, we applied 2, 3 and 6 stimuli at frequencies of 20, 40 and 100 Hz to elicit AP-mediated Glu release. At all frequencies tested, Small/IT and Large/PT terminals exhibited opposite types of short-term plasticity, i.e. depression in IT and potentiation in PT terminals (Tab. 1 and Fig. 2*A*-*E*). In general, the peak and maximal amplitudes observed after stimulus #6 (normalized to response #1) were higher after 100 vs. 20 Hz, and larger in PT than IT terminals (Tab. 1, Fig. 2*E*). The TauD values, as derived from the first term of a double exponential fitting curve after stimulus #6 (double arrow in Fig. 2D), exhibited little sensitivity to repetitive activation up to 100 Hz, (Fig. 2*F*), but the Spread of the $iGlu_u$ signals increased with repetitive stimulation at 100 Hz, notably at PT terminals (Fig. 2*G*). PT terminals also accumulated larger amounts of residual $iGlu_u$ fluorescence (Fig. 2*H*), as defined by fitting a double exponential function to the #6 decay (Fig. 2*D*). The data suggests that the stimulus-locked response to the last AP adds to incompletely cleared Glu. Accordingly, the integral $iGlu_u$ fluorescence produced by 6 pulses at 100 Hz was significantly larger in PT terminals (Fig. 2*I*). Thus, under repetitive activation conditions, large PT corticostriatal terminals might be more affected by conditions of weak astrocytic Glu uptake.

Directly induced Glu transients in tetrodotoxin (TTX)

With the AP mechanism intact, fluorescence might also originate from neighbouring release sites, especially if the axon heads deeper into the z-plane of the slice. In case of the serial (*en passant*) type synapses (as characteristic of PT afferents) this could erroneously increase signal duration and spread. Another caveat to be faced in

the case of HD preparations is a possible alteration of voltage-activated channels in the cortical afferents (Silva et al., 2017) which may affect the duration of the presynaptic depolarization, the influx of Ca^{2+} and, consequently, the amplitude and duration of $iGlu_u$ signals, without having a direct impact on the clearance machinery of the astrocytes. Moreover, respective deficits might preferentially occur in IT or PT axons. Considering these complexities it was decided to by-pass the AP mechanism by directly depolarizing the glutamatergic terminals in TTX and to perform the following measurements solely in PT synapses.

To achieve in TTX [Glu] elevations similar to those obtained under physiological activation conditions from PT terminals at 100 Hz, it was sufficient to increase $[Ca^{2+}]_{ec}$ to 5 mM and to add a hyperpolarizing prepulse to the standard 1 ms depolarization used both in AP and TTX experiments. In the absence of a conditioning hyperpolarizing prepulse, the direct depolarization was insufficient to elicit release (Fig. 3*A*). The results of Fig. 3*B-D* indicate that the selected protocol provided a good match between the physiologically induced #6 responses at 100 Hz and the directly induced responses in TTX. In any case, $iGlu_u$ elevations were completely abolished by the Ca^{2+} channel blocker Cd^{2+} (Fig. 3*E*). This stimulation protocol was then expected to provide a reasonably standardized single terminal activation for assessing the Glu uptake of WT vs. HD mice.

Slowed Glu clearance at single PT-type corticostriatal terminals in HD

In the Q175 mouse model of HD, motor symptoms (hypo- and dyskinesia, pathological circling) develop quite slowly. However, at the age of one year and older, both Q175 HET and HOM resemble the human phenotype in the manifest phase (Khakh et al., 2017). In Q175 HOM motor impairment coincided with the appearance of pathological gamma oscillations in the local field potential (LFP) recordings at quiet rest (Rothe et al., 2015). In R6/2 mice, the changes in the LFP power spectrum were less pronounced after treatment with ceftriaxone (CEF), a transcriptional activator reported to increase the level of EAAT2 protein in the dorsal striatum (Miller et al., 2012).

Fig. 4*A* shows representative amplitude-scaled specimen records for the three test groups illustrating our main finding: In HD slices the $iGlu_u$ transients decayed more slowly (link to video: https://neurophysiology-grantyn.charite.de/video/Q175_iGluSnFr-ultrafast_WT_HET_HOM_2fps.ogg). Interestingly, this HD-related alteration was not only present in Q175 HOM but also in HET (Fig. 4*B*) thereby underlining the usefulness of the Q175 mouse model for research on HD pathology and therapy.

An important additional question concerns the amount of released Glu. Is it larger in HD mice? This was not the case, on the contrary. With respect to WT, Q175 HET and HOM exhibited a significant deficit in the peak ΔF/F values (Tab. 2, Fig. 4*C*). This result is in line with the data from R6/2 (Parievsky et al., 2017) suggesting that the presently disclosed HD-related prolongation of the $iGlu_u$ signal occurs despite a concomitant decrease in the Glu output from single PT terminals.

Nevertheless, the above observations do not immediately prove that the prolongation of the ΔF/F transient is due to an altered functionality of the astrocytes. It was at least necessary to clarify whether TauD values responded to pharmacological manipulation of astrocytic Glu transport. This was the case. The $iGlu_u$ transients of PT terminals exhibited a clear sensitivity to TFB-TBOA (Fig. 4*D*). In WT, 100 nM of the antagonist prolonged the $iGlu_u$ decay to the same extent as the disease, the effect of pharmacological EAAT2 block being less pronounced in Q175 HOM (Fig. 4*E, F*).

Although $iGlu_u$ expression in the presynaptic terminals cannot provide exhausting information on the spatial characteristics of perisynaptic [Glu], it should be noted that the “Spread” (black outlines in Fig. 4*G*) was also increased, reaching 1.61± 0.14 µm (n=19) in HOM (Tab. 2). According to the presently available models of glutamatergic synapses (Zheng et al., 2008; Scimemi and Beato, 2009), this should be sufficient to activate extrasynaptic NMDA receptors.

The pixels with the highest ΔF/F were always located next to the outline of the resting terminal (see Fig. 1*D*). The decay from the maximal amplitude next to the active zone

thereby was used to estimate clearance at the site of release minimizing the influence of Glu diffusion. The graphs of Fig. 5*A-C* show the ranges of maximal amplitudes and TauD and reveal the synaptic symptoms of HD on first glance: i.e. a decrease in the range of maximal amplitudes next to the source of Glu elevation and an increase in the range of TauD. As a first approximation, one can state that in Q175 HET 30% of the synapses (19/68) were sick, the present exclusion criterion from the group of healthy synapses being TauD >= 10 ms and/or maximal $\Delta F/F$ <200%.

Positive correlation between Glu release and clearance in HD but not WT synapses

In the case that the density of astrocytic Glu transporters next to the site of release is compromised by HD, more distantly located transporters could come into play which might be reflected by a positive correlation between TauD and peak amplitudes derived from fluctuating responses generated by a given synapse. To eliminate the impact of inter-synapse variability in favour of an analysis of inter-trial variability we plotted the respective PPR values, i.e. examined the normalized 2nd responses (Fig. 5*D-F*). This approached revealed that in HD but not WT synapses larger [Glu] elevations indeed required longer time for clearance which suggests that in HD Glu may find its astrocytic transporter at bigger distance, in line with recent FRET data from corticostriatal synapses in R6/2 (Octeau et al., 2018).

Prolonged NMDAR components of unitary EPSCs in HD

NMDARs are sensitive indicators of [Glu] and therefore well suited to detect a potentially existing Glu clearance deficiency in the environment of active synapses, provided that the analysed responses are derived from one or few synapses only (Chiu and Jahr, 2017). Here we used focal optical activation of individual corticostriatal axons to record uEPSCs at -70 and +50 mV. The experiments showed (Tab. 3) that the T50 value of the uEPSC recorded at +50 mV is i) solely dependent on NMDARs, ii) prolonged in Q175 HD and iii) recovered to WT levels after treatment with CEF suggesting a sensitivity of corticostriatal input to the level of EAAT2 expression (Tab. 3, Fig. 6*A-F*). There also was an increase in the peak amplitudes of the uEPSCs recorded both at +50 mV and -70 mV which may, at least in part, reflect

reduced lower failure rate due to more efficient ChR-mediated depolarization of the stimulated axons. In accordance with this idea, not only the failure rate but also the coefficient of variation (CV) of the AMPA response at -70 was found to be smaller in HD (Fig. 6*E*, *F*). In any case, these results are in line with the concept that HD slows glutamate clearance.

Reduced perisynaptic EAAT2 protein at corticostriatal terminals

To clarify whether the observed clearance deficit is indeed accompanied by a reduction of EAAT2 protein levels in the environment of corticostriatal terminals, we performed a quantification of EAAT2 IF in small ROIs centred to single vGluT1-positive terminals of fixed sections (Fig. 7*A*-*E*). These experiments revealed a small (-15%) but significant HD-dependent decrease in the mean intensity of supra-threshold EAAT2+ pixels, along with a significant (-13%) decrease in the size of the EAAT+ area.

DISCUSSION

The analysis of single synapse $iGlu_u$ transients in acute slice preparations from adult mice provides new information on Glu clearance in its relation to the respective transmitter load. To summarize: 1) The peak [Glu] elevations produced by PT and IT terminals differed significantly (factor 5:1). 2) However, throughout the Glu challenges tested in normal mice, both types of synapses coped with the induced [Glu] elevations (did not show much increase of TauD even at 100 Hz activation), although the Spread and the residual $iGlu_u$ fluorescence increased with increasing peak amplitudes, notably at PT terminals. 3) HD decreased the range of maximal amplitudes but increased the range of TauD. About one third of the synapses tested in Q175 HET were diagnosed with a functional defect, based on the time needed for Glu clearance (Tau D of $iGlu_u$ >= 10 ms) and/or the amount of released Glu (maximal $\Delta F/F$ <= 200%). 4) The responses to paired (Δt=50 ms) activation at 0.1 Hz exhibited some inter-trial variabilty of the #2 responses. This analysis revealed a disease-related loss of independence between the indicators of uptake on release. In Q175 HET but not WT, larger individual responses were associated with larger TauD. 5) The NMDAR-mediated unitary EPSCs elicited by optical stimulation of single ChR-

expressing corticostriatal axons were prolonged in Q175 HOM. 5) Also in Q175 HOM, less EAAT2 was found in the environment of corticostriatal terminals.

PT versus IT terminals

The unexpected differences in the properties of PT vs. IT terminals raise further questions on the mechanism(s) of release plasticity of the glutamatergic afferents to the dorsal striatum. Previous electrophysiological studies (Ding et al., 2008) implied that corticostriatal connections preferentially exhibit paired pulse facilitation (PPF) while thalamostriatal connections are prone to paired pulse depression (PPD). Our results confirm preferential PPF with regard to the PT subgroup of corticostriatal afferents under physiological activation conditions (Tab. 1). However, as in any other synapse (for instance (Kirischuk et al., 2002)), a conversion from PPF to PPD is easily achieved by increasing the Ca^{2+} influx. There is a widely accepted rule of thumb suggesting that smaller initial responses are likely to produce facilitation in subsequent responses, and *vice versa*. Considering that under the same experimental conditions PT and IT terminals produced about the same initial Glu output, but opposite types of plasticity, one can assume that these terminals indeed represent two classes of afferents with some differences in the presynaptic control of transmitter release.

Under condition of repetitive activation the size of synaptic terminals and associated differences in the vesicle pool size could affect the integral Glu output, but also the degree of Glu escape (Genoud et al., 2006; Bernardinelli et al., 2014; Medvedev et al., 2014; Gavrilov et al., 2018). It has been hypothesized that thicker terminals could push the PAPs further away from the site of exocytosis which may result in wider signal spread if the transporters are challenged with a pronounced build-up of [Glu] as found in PT terminals.

The hypothesis of non-saturating Glu uptake in healthy glutamatergic synapses

In view of a long history of changing opinions on the significance of astrocytic Glu transport as a possible determinant of synaptic strength it is good to have new tools at hand to shed light on the possible limits of Glu clearance in health and disease.

Our uEPSC data from synaptic connections with one or few terminals confirm the long-standing idea that a weakness of Glu uptake has little influence on the decay kinetics of the fast desensitizing AMPA responses (Hestrin et al., 1990; Asztely et al., 1997; Goubard et al., 2011; Campbell et al., 2014). Moreover, our $iGlu_u$ data from healthy mice are in line with the more controversial prediction that in “normal” glutamatergic synapses glutamate transport would cope with any amount of physiologically released Glu (Diamond and Jahr, 2000; Tzingounis and Wadiche, 2007). Nevertheless, the present $iGlu_u$-based postulate of non-saturating Glu uptake for IT- and PT-type corticostriatal synapses will need further verification under a wider range of conditions. It was already shown that the state of astrocytes could affect the structural plasticity of PAPs (Theodosis et al., 2008; Reichenbach et al., 2010; Bernardinelli et al., 2014; Heller and Rusakov, 2015; Verkhratsky and Nedergaard, 2018). Activity- and disease-dependent PAP retraction could then produce a large variety of spill-out and spill-in effects which may not only change the access of the available transmitter(s) to respective neuronal and glial receptors, but also influence the efficacy of the astrocytic transport machinery itself (Armbruster et al., 2016).

Evidence for impairment of Glu clearance in HD

Symptomatic HD is characterized by the loss of glutamatergic terminals in the dorsal striatum but it is still not clear whether this disease-related process of synapse pruning is to be attributed to glutamate excitotoxicity (Reiner and Deng, 2018). While the long-term consequences of reduced Glu clearance remain to be clarified, our present experiments provide new evidence suggesting that in symptomatic Q175 mice a significant fraction of PT synapses is afflicted by the disease, most likely exhibiting alterations in both uptake and release. When normalizing the fluctuating $iGlu_u$ amplitudes generated in the course of repeated activation of the same synapse, it turned out that HD but not WT synapses displayed a positive, presumably pathological correlation between TauD and maximal $\Delta F/F$ amplitudes. In view of the observed TBOA effects and the decrease of perisynaptic EAAT2 protein, it seems very likely that the observed synapse pathology is associated with the expression of *mHTT* in astrocytes (Faideau et al., 2010).

How do the present results obtained with $iGlu_u$ in the HD striatum relate to synaptic properties outlined by more conventional electrophysiological approaches? The results on $iGlu_u$ Spread are in line with the prolonged NMDAR activation revealed in the uEPSCs experiments of Q175 HOM. However, the slight but significant increase of uEPSC amplitudes will need a verification with other single axon stimulation techniques. Previous experiments with minimal electrical stimulation (Rothe et al., 2015) pointed to a decreased range of uEPSC amplitudes, as expected in the case of reduced number of Glu-releasing sites or smaller vesicle pools.

Considering the novelty of the present approach, it is not surprising that some results from other labs were not confirmed, in particular those obtained with the slow Glu indicator iGluSNFR (Marvin et al., 2013). (Parsons et al., 2016) activated glutamate release by high frequency electrical field stimulation and used the iGluSnFR sensor to record Glu elevations in large viewfields. They found no HD-related difference in the fluorescence decay, in contrast to (Jiang et al., 2016). Both studies were carried out in R6/2 mice, the main difference being in the expression of the Glu sensor in neurons vs. astrocytes. (Parievsky et al., 2017) applied optical field stimulation of channel-rhodopsin-(ChR2(H134R))-expressing corticostriatal axons to induce EPSCs in SPNs.. This approach showed no increase in the decay times (T90-10) of NMDAR-mediated currents. On the contrary, the latter were significantly shorter in HD. However, considering the mean T90-10 values of this study (~750 ms) it seems possible that the asynchrony of release characteristic of this type of optical field stimulation may not give the resolution needed for the estimation of synaptic Glu clearance. In general, space- and volume-averaging effects resulting from bulk activation of synaptic and non-synaptic Glu release and low resolution of the electrical or fluorescent signals can be expected to influence the interpretation of results on Glu uptake and release (see (Jensen et al., 2017; Reynolds et al., 2018) for a concise summary on these issues).

The ultimate prove of Glu uptake deficiency as a cause of synapse pathology in the dorsal striatum will be the recovery of normal synaptic performance after a therapeutic intervention targeting the astrocytes. Functional benefits from CEF injections have already been reported (Miller et al., 2008; Miller et al., 2012) and were

attributed to a enhanced EAAT2 expression in astroglia. Attempts to achieve beneficial effects by injecting recombinant astrocyte-targeting AAV8-EAAT2 constructs failed in a SOD1 mouse model of amyotrophic lateral sclerosis (Li et al., 2015) but were successful in reversing established neuropathic pain behavior (Falnikar et al., 2016). Most intriguing, intrastriatal injection of a recombinant viral Kir4.1 vector restored a normal level of EAAT2 protein (Tong et al., 2014). However, it is not yet clear whether a mere stimulation of EAAT2 expression would suffice to achieve the desired reversal of motor symptoms in HD, because synaptic targeting and the activity of Glu transporters are also influenced by local translation (Sakers et al., 2017), lateral mobility (Murphy-Royal et al., 2015) and internalization (Leinenweber et al., 2011; Ibanez et al., 2016). Clearly, much more information is needed to understand the regulation of Glu uptake in the context of other astrocytic signaling cascades.

Conclusion

Achievement of normal EAAT2 function should remain a major goal in the therapy of HD.

FIGURE LEGENDS

Fig. 1. Monitoring single synapse Glu transients in acute slices from adult mice after expression of the genetically encoded ultrafast Glu sensor $iGlu_u$ in corticostriatal neurons. *(A)* Resting $iGlu_u$ fluorescence merged to the respective 63x DIC image of a corticostriatal slice showing an axon with 3 adjacent varicosities and a stimulation pipette at the central bouton. *(B)* Simplified scheme of the corticostriatal circuitry (Reiner et al., 2010), illustrating the concept of preferential projection of pyramidal tract (PT) neurons to indirect pathway striatal projection neurons (iSPNs) and intratelencephalic (IT) neurons to direct pathway SPNs (dSPNs) and size-differences between the IT and PT terminals. Bimodal distribution of bouton diameters as determined by the supra-threshold resting fluorescence before stimulation. Boutons with diameter >= 0.63 µm were defined as “Large” and assumed to be issued by PT axons. *(D)* Example of a type PT bouton with the respective $iGlu_u$ fluorescence at rest (left) and at the peak of an AP-mediated $iGlu_u$ response (right). *(E)* $iGlu_u$ responses recorded from the bouton shown in *(A, D)*. Experiment in 2 mM Ca^{2+} and 1 mM Mg^{2+}.

Simultaneous recording of stimulation current (upper trace), mean supra-threshold pixel intensity (middle trace) and the area of supra-threshold pixels (bottom trace). A monoexponential function is fitted to the decay of the 1st (#1) iGlu$_u$ transient with the respective time constants shown next to the fitting curves. *(F)* Positive correlation between the "Spread" at the time of peak and TauD after stimulus #1. *(G)* Peak amplitudes of responses to stimulus #1. There is no difference between small and large terminals. *(H) S*ignificant correlation between the PPR of peak amplitudes and bouton diameter for single or #1 stimuli.

Fig. 2. Contrasting dynamics of Glu release from small and large corticostriatal terminals. *(A-D)* Specimen records of AP-mediated iGlu$_u$ signals at 20 and 100 Hz, as derived from small and large boutons. All iGlu$_u$ transients were elicited in an AP-dependent manner in 2 mM Ca^{2+}. Experimental conditions as in Fig. 1. (*E-I*) Quantification of results. The large terminals produced a significant build-up of residual iGlu$_u$ fluorescence (single arrow) that added to the fast stimulus-locked transients (double arrow). Note that the time integral of all supra-threshold pixel intensities generated by a 6-pulse train at 100 Hz during a sampling period of 70 ms was much bigger in large boutons *(I)*.

Fig. 3. Responses to directly induced test pulses by-passing the AP mechanism in WT boutons of type P. *(A)* Experiment in elevated $[Ca^{2+}]_{ec}$. Left: Response to electrical stimulation in the absence of TTX elicited by a short (1 ms) depolarizing pulse. In 5 mM Ca^{2+} the AP-mediated response exhibits paired pulse depression. Middle: same condition but in the presence of TTX. Note complete block of Glu release. Right: Response in 5 mM Ca^{2+} and TTX, but elicited with the 1 ms depolarizing pulse preceded by a short hyperpolarizing pulse, to recruit additional Ca^{2+} channels. *(B)* Stimulus intensity for direct activation of Glu release was adjusted such that the amplitudes of iGlu$_u$ signals matched the amplitudes observed with the last (#6) stimulus in a 100 Hz train under physiological conditions (2 mM Ca^{2+} and intact AP generation). *(C, D)* Lack of differences between physiological and test pulse-induced responses. *(E)* The directly induced responses were completely blocked by Cd^{2+} (500 μM).

Fig. 4. HD-related differences in the clearance of synaptically released Glu. *(A)* Specimen records of $iGlu_u$ responses to direct activation of a P-type varicosity in the presence of TTX. Fitting a monoexponential function to the decay of the $iGlu_u$ transient of Q175 WT (green), HET (orange) and HOM (red) revealed differences in the duration of the Glu transient. The amplitudes were normalized to the same peak value. *(B, C)* Quantification of the results from WT (green), HET (orange) and HOM (red). *(D-F)* Incubation of WT slices in 100 nM of TFB-TBOA simulated the depression of Glu clearance observed in HOM. *(G, H)* Specimen images and traces, showing the "Spread" in WT and HD mice. *(I, J)* Quantification of results from analysis of the $iGlu_u$ signals in WT and HD mice. The "Spread" in (I) refers to the diameter of the supra-threshold pixel area approximated as a circle in the X-Y plane.

Fig. 5. HD-related differences in Glu release and uptake. (*A-C*) Correlograms of TauD and maximal ΔF/F amplitudes in WT (*A*) and in Q175 HET (*B, C*). To emphasize the HD-related differences in the range of obtained values, the data points were boxed green in WT and red in Q175 HET. (*D-F*) Correlograms of TauD and peak amplitudes of ΔF/F. To eliminate inter-synapse variability, #2 responses were normalized to #1 responses. The inter-trial variability of responses elicited at a repetition frequency of 0.1 Hz was used to test for a positive correlation between TauD and peak amplitudes of ΔF/F. Note positive correlation in HET (*F*) but not WT (*D, E*). Data from HET: 11 animals, 23 synapses, 3 trials per synapse.

Fig. 6. HD-related prolongation of the NMDAR component in uEPSCs elicited by optical stimulation of single corticostriatal afferents visualized by EYFP fluorescence after the expression of CaMKIIa.hChR2(E123T/T159C)-EYFP.hGH. *(A)* Specimen traces as recorded at two different holding potentials in the presence of bicuculline methiodide (25 μM). *(B)* Same traces as *(A)* but aligned to peak. See prolonged decay in comparison with records at -70 mV. This difference was abolished by APV (not illustrated), and more pronounced in Q175 HOM (red traces). Treatment with CEF abolished the uEPSC prologation at +50 mV (blue traces). *(C-F)* Quantification of results. Note significantly larger T50 values of the NMDAR-mediated response at +50 mV and recovery after CEF treatment *(C)*.

Fig. 7. Lower than in WT perisynaptic EAAT2 immunofluorescence in Q175 HOM. *(A)* Merged image of a view-field in the dorsal striatum showing the vGluT1 IF of corticostriatal synaptic terminals (green) and EAAT2 IF clusters (red) in the immediate vicinity of vGLUT+ terminals and in contact with a blood vessel (arrow). *(B-C)* Enlarged images of the (ROI) boxed in *(A)*, with separate *(B, C)* and merged *(D)* channels. *(E)* Pixels with supra-threshold EAAT2 IF (light blue). (*F, G*) Mean intensity and area of supra-threshold pixels in the dorsal striatum of WT and Q175 HOM. Numbers refer to the number of ROIs, each comprising one vGluT1+ varicosity. Data from 4 WT and 4 Q175 HOM.

REFERENCES

Armbruster M, Hanson E, Dulla CG (2016) Glutamate clearance is locally modulated by presynaptic neuronal activity in the cerebral cortex. J Neurosci 36: 10404-10415.

Asztely F, Erdemli G, Kullmann DM (1997) Extrasynaptic glutamate spillover in the hippocampus: dependence on temperature and the role of active glutamate uptake. Neuron 18: 281-293.

Barbour B (2001) An evaluation of synapse independence. J Neurosci 21: 7969-7984.

Behrens PF, Franz P, Woodman B, Lindenberg KS, Landwehrmeyer GB (2002) Impaired glutamate transport and glutamate-glutamine cycling: downstream effects of the Huntington mutation. Brain 125: 1908-1922.

Bergles DE, Diamond JS, Jahr CE (1999) Clearance of glutamate inside the synapse and beyond. Curr Opin Neurobiol 9: 293-298.

Bernardinelli Y, Muller D, Nikonenko I (2014) Astrocyte-synapse structural plasticity. Neural Plast 2014: 232105; epub.

Bradford J, Shin JY, Roberts M, Wang CE, Li XJ, Li S (2009) Expression of mutant huntingtin in mouse brain astrocytes causes age-dependent neurological symptoms. Proc Natl Acad Sci U S A 106: 22480-22485.

Cahoy JD, Emery B, Kaushal A, Foo LC, Zamanian JL, Christopherson KS, Xing Y, Lubischer JL, Krieg PA, Krupenko SA, Thompson WJ, Barres BA (2008) A transcriptome database for astrocytes, neurons, and oligodendrocytes: a new resource for understanding brain development and function. J Neurosci 28: 264-278.

Campbell SL, Hablitz JJ, Olsen ML (2014) Functional changes in glutamate transporters and astrocyte biophysical properties in a rodent model of focal cortical dysplasia. Front Cell Neurosci 8: 425.

Chiu DN, Jahr CE (2017) Extracellular glutamate in the nucleus accumbens is nanomolar in both synaptic and non-synaptic compartments. Cell Rep 18: 2576-2583.

Deng YP, Wong T, Bricker-Anthony C, Deng B, Reiner A (2013) Loss of corticostriatal and thalamostriatal synaptic terminals precedes striatal projection neuron pathology in heterozygous Q140 Huntington's disease mice. Neurobiol Dis 60: 89-107.

Diamond JS, Jahr CE (2000) Synaptically released glutamate does not overwhelm transporters on hippocampal astrocytes during high-frequency stimulation. J Neurophysiol 83: 2835-2843.

Ding J, Peterson JD, Surmeier DJ (2008) Corticostriatal and thalamostriatal synapses have distinctive properties. J Neurosci 28: 6483-6492.

Dvorzhak A, Gertler C, Harnack D, Grantyn R (2013a) High frequency stimulation of the subthalamic nucleus leads to presynaptic GABA(B)-dependent depression of subthalamo-nigral afferents. PLoS One 8: e82191.

Dvorzhak A, Semtner M, Faber DS, Grantyn R (2013b) Tonic mGluR5/CB1-dependent suppression of inhibition as a pathophysiological hallmark in the striatum of mice carrying a mutant form of huntingtin. J Physiol 591: 1145-1166.

Dvorzhak A, Vagner T, Grantyn R (2016) Functional indicators of glutamate transport in single striatal astrocytes and the influence of Kir4.1 in normal and Huntington mice. J Neurosci 16: 4959-4975.

Faideau M, Kim J, Cormier K, Gilmore R, Welch M, Auregan G, Dufour N, Guillermier M, Brouillet E, Hantraye P, Deglon N, Ferrante RJ, Bonvento G (2010) In vivo expression of polyglutamine-expanded huntingtin by mouse striatal astrocytes impairs glutamate transport: a correlation with Huntington's disease subjects. Hum Mol Genet 19: 3053-3067.

Falnikar A, Hala TJ, Poulsen DJ, Lepore AC (2016) GLT1 overexpression reverses established neuropathic pain-related behavior and attenuates chronic dorsal horn neuron activation following cervical spinal cord injury. Glia 64: 396-406.

Gavrilov N, Golyagina I, Brazhe A, Scimemi A, Turlapov V, Semyanov A (2018) Astrocytic coverage of dndritic spines, dendritic shafts, and axonalboutons in hippocampal neuropil. Front Cell Neurosci 12: 248.

Genoud C, Quairiaux C, Steiner P, Hirling H, Welker E, Knott GW (2006) Plasticity of astrocytic coverage and glutamate transporter expression in adult mouse cortex. PLoS Biol 4: e343.

Goubard V, Fino E, Venance L (2011) Contribution of astrocytic glutamate and GABA uptake to corticostriatal information processing. J Physiol 589: 2301-2319.

Grewer C, Gameiro A, Rauen T (2014) SLC1 glutamate transporters. Pflugers Arch 466: 3-24.

Helassa N, Durst CD, Coates C, Kerruth S, Arif U, Schulze C, Wiegert JS, Geeves M, Oertner TG, Torok K (2018) Ultrafast glutamate sensors resolve high-frequency release at Schaffer collateral synapses. Proc Natl Acad Sci U S A 115: 5594-5599.

Heller JP, Rusakov DA (2015) Morphological plasticity of astroglia: Understanding synaptic microenvironment. Glia 63: 2133-2151.

Hestrin S, Sah P, Nicoll RA (1990) Mechanisms generating the time course of dual component excitatory synaptic currents recorded in hippocampal slices. Neuron 5: 247-253.

Huang K, Kang MH, Askew C, Kang R, Sanders SS, Wan J, Davis NG, Hayden MR (2010) Palmitoylation and function of glial glutamate transporter-1 is reduced in the YAC128 mouse model of Huntington disease. Neurobiol Dis 40: 207-215.

Ibanez I, Diez-Guerra FJ, Gimenez C, Zafra F (2016) Activity dependent internalization of the glutamate transporter GLT-1 mediated by beta-arrestin 1 and ubiquitination. Neuropharmacology 107: 376-386.

Jensen TP, Zheng K, Tyurikova O, Reynolds JP, Rusakov DA (2017) Monitoring single-synapse glutamate release and presynaptic calcium concentration in organised brain tissue. Cell Calcium 64: 102-108.

Jiang R, Diaz-Castro B, Looger LL, Khakh BS (2016) Dysfunctional calcium and glutamate signaling in striatal astrocytes from Huntington's disease model mice. J Neurosci 36: 3453-3470.

Khakh BS, Beaumont V, Cachope R, Munoz-Sanjuan I, Goldman SA, Grantyn R (2017) Unravelling and exploiting astrocyte sysfunction in Huntington's disease. Trends Neurosci 40: 422-437.

Kincaid AE, Zheng T, Wilson CJ (1998) Connectivity and convergence of single corticostriatal axons. J Neurosci 18: 4722-4731.

Kirischuk S, Clements JD, Grantyn R (2002) Presynaptic and postsynaptic mechanisms underlie paired pulse depression at single GABAergic boutons. J Physiol 543: 99-116.

Kirischuk S, Veselovsky N, Grantyn R (1999) Relationship between presynaptic calcium transients and postsynaptic currents at single gamma-aminobutyric acid (GABA)ergic boutons. Proc Natl Acad Sci U S A 96: 7520-7525.

Lehre KP, Danbolt NC (1998) The number of glutamate transporter subtype molecules at glutamatergic synapses: Chemical and stereological quantification in young adult rat brain. J Neurosci 18: 8751-8757.

Leinenweber A, Machtens JP, Begemann B, Fahlke C (2011) Regulation of glial glutamate transporters by C-terminal domains. J Biol Chem 286: 1927-1937.

Li K, Hala TJ, Seetharam S, Poulsen DJ, Wright MC, Lepore AC (2015) GLT1 overexpression in SOD1(G93A) mouse cervical spinal cord does not preserve diaphragm function or extend disease. Neurobiol Dis 78: 12-23.

Lievens JC, Woodman B, Mahal A, Spasic-Boscovic O, Samuel D, Kerkerian-Le Goff L, Bates GP (2001) Impaired glutamate uptake in the R6 Huntington's disease transgenic mice. Neurobiol Dis 8: 807-821.

Marcaggi P, Attwell D (2004) Role of glial amino acid transporters in synaptic transmission and brain energetics. Glia 47: 217-225.

Marvin JS, Borghuis BG, Tian L, Cichon J, Harnett MT, Akerboom J, Gordus A, Renninger SL, Chen TW, Bargmann CI, Orger MB, Schreiter ER, Demb JB, Gan WB,

Hires SA, Looger LL (2013) An optimized fluorescent probe for visualizing glutamate neurotransmission. Nat Methods 10: 162-170.

Medvedev N, Popov V, Henneberger C, Kraev I, Rusakov DA, Stewart MG (2014) Glia selectively approach synapses on thin dendritic spines. Philos Trans R Soc Lond B Biol Sci 369: 20140047.

Melone M, Bellesi M, Ducati A, Iacoangeli M, Conti F (2011) Cellular and synaptic localization of EAAT2a in human cerebral cortex. Front Neuroanat 4: 151.

Menalled LB, Kudwa AE, Miller S, Fitzpatrick J, Watson-Johnson J, Keating N, Ruiz M, Mushlin R, Alosio W, McConnell K, Connor D, Murphy C, Oakeshott S, Kwan M, Beltran J, Ghavami A, Brunner D, Park LC, Ramboz S, Howland D (2012) Comprehensive behavioral and molecular characterization of a new knock-in mouse model of Huntington's disease: zQ175. PLoS One 7: e49838.

Meunier C, Merienne N, Jolle C, Deglon N, Pellerin L (2016) Astrocytes are key but indirect contributors to the development of the symptomatology and pathophysiology of Huntington's disease. Glia 64: 1841-1856.

Miller BR, Dorner JL, Bunner KD, Gaither TW, Klein EL, Barton SJ, Rebec GV (2012) Up-regulation of GLT1 reverses the deficit in cortically evoked striatal ascorbate efflux in the R6/2 mouse model of Huntington's disease. J Neurochem 121: 629-638.

Miller BR, Dorner JL, Shou M, Sari Y, Barton SJ, Sengelaub DR, Kennedy RT, Rebec GV (2008) Up-regulation of GLT1 expression increases glutamate uptake and attenuates the Huntington's disease phenotype in the R6/2 mouse. Neurosci 153: 329-337.

Murphy-Royal C, Dupuis JP, Varela JA, Panatier A, Pinson B, Baufreton J, Groc L, Oliet SH (2015) Surface diffusion of astrocytic glutamate transporters shapes synaptic transmission. Nat Neurosci 18: 219-226.

Nahir B, Jahr CE (2013) Activation of extrasynaptic NMDARs at individual parallel fiber-molecular layer interneuron synapses in cerebellum. J Neurosci 33: 16323-16333.

Nedergaard M, Verkhratsky A (2012) Artifact versus reality--how astrocytes contribute to synaptic events. Glia 60: 1013-1023.

Octeau JC, Chai H, Jiang R, Bonanno SL, Martin KC, Khakh BS (2018) An optical neuron-astrocyte proximity assay at synaptic distance scales. Neuron 98: 49-66.

Papouin T, Dunphy J, Tolman M, Foley JC, Haydon PG (2017) Astrocytic control of synaptic function. Philos Trans R Soc Lond B Biol Sci 372: 20160154.

Parievsky A, Moore C, Kamdjou T, Cepeda C, Meshul CK, Levine MS (2017) Differential electrophysiological and morphological alterations of thalamostriatal and corticostriatal projections in the R6/2 mouse model of Huntington's disease. Neurobiol Dis 108: 29-44.

Parsons MP, Vanni MP, Woodard CL, Kang R, Murphy TH, Raymond LA (2016) Real-time imaging of glutamate clearance reveals normal striatal uptake in Huntington disease mouse models. Nat Commun 7: 11251.

Pekny M, Pekna M, Messing A, Steinhauser C, Lee JM, Parpura V, Hol EM, Sofroniew MV, Verkhratsky A (2016) Astrocytes: a central element in neurological diseases. Acta Neuropathol 131: 323-345.

Reichenbach A, Derouiche A, Kirchhoff F (2010) Morphology and dynamics of perisynaptic glia. Brain Res Rev 63: 11-25.

Reiner A, Deng YP (2018) Disrupted striatal neuron inputs and outputs in Huntington's disease. CNS Neurosci Ther 24: 250-280.

Reiner A, Hart NM, Lei W, Deng Y (2010) Corticostriatal projection neurons - dichotomous types and dichotomous functions. Front Neuroanat 4: 142.

Reynolds JP, Zheng K, Rusakov DA (2018) Multiplexed calcium imaging of single-synapse activity and astroglial responses in the intact brain. Neurosci Lett 10.

Rose CR, Felix L, Zeug A, Dietrich D, Reiner A, Henneberger C (2018) Astroglial Glutamate Signaling and Uptake in the Hippocampus. Front Mol Neurosci 10: 451.

Rothe T, Deliano M, Wojtowicz AM, Dvorzhak A, Harnack D, Paul S, Vagner T, Melnick I, Stark H, Grantyn R (2015) Pathological gamma oscillations, impaired dopamine release, synapse loss and reduced dynamic range of unitary glutamatergic synaptic transmission in the striatum of hypokinetic Q175 Huntington mice. Neurosci 311: 519-538.

Sakers K, Lake AM, Khazanchi R, Ouwenga R, Vasek MJ, Dani A, Dougherty JD (2017) Astrocytes locally translate transcripts in their peripheral processes. Proc Natl Acad Sci U S A 114: E3830-E3838.

Scimemi A, Beato M (2009) Determining the neurotransmitter concentration profile at active synapses. Mol Neurobiol 40: 289-306.

Shin JY, Fang ZH, Yu ZX, Wang CE, Li SH, Li XJ (2005) Expression of mutant huntingtin in glial cells contributes to neuronal excitotoxicity. J Cell Biol 171: 1001-1012.

Silva FR, Miranda AS, Santos RPM, Olmo IG, Zamponi GW, Dobransky T, Cruz JS, Vieira LB, Ribeiro FM (2017) N-type Ca(2+) channels are affected by full-length mutant huntingtin expression in a mouse model of Huntington's disease. Neurobiol Aging 55: 1-10.

Theodosis DT, Poulain DA, Oliet SH (2008) Activity-dependent structural and functional plasticity of astrocyte-neuron interactions. Physiol Rev 88: 983-1008.

Tong X, Ao Y, Faas GC, Nwaobi SE, Xu J, Haustein MD, Anderson MA, Mody I, Olsen ML, Sofroniew MV, Khakh BS (2014) Astrocyte Kir4.1 ion channel deficits contribute to neuronal dysfunction in Huntington's disease model mice. Nat Neurosci 17: 694-703.

Tzingounis AV, Wadiche JI (2007) Glutamate transporters: confining runaway excitation by shaping synaptic transmission. Nat Rev Neurosci 8: 935-947.

Verkhratsky A, Nedergaard M (2018) Physiology of astroglia. Physiol Rev 98: 239-389.

Verkhratsky A, Zorec R, Rodriguez JJ, Parpura V (2016) Astroglia dynamics in ageing and Alzheimer's disease. Curr Opin Pharmacol 26: 74-79.

Zheng K, Scimemi A, Rusakov DA (2008) Receptor actions of synaptically released glutamate: the role of transporters on the scale from nanometers to microns. Biophys J 95: 4584-4596.

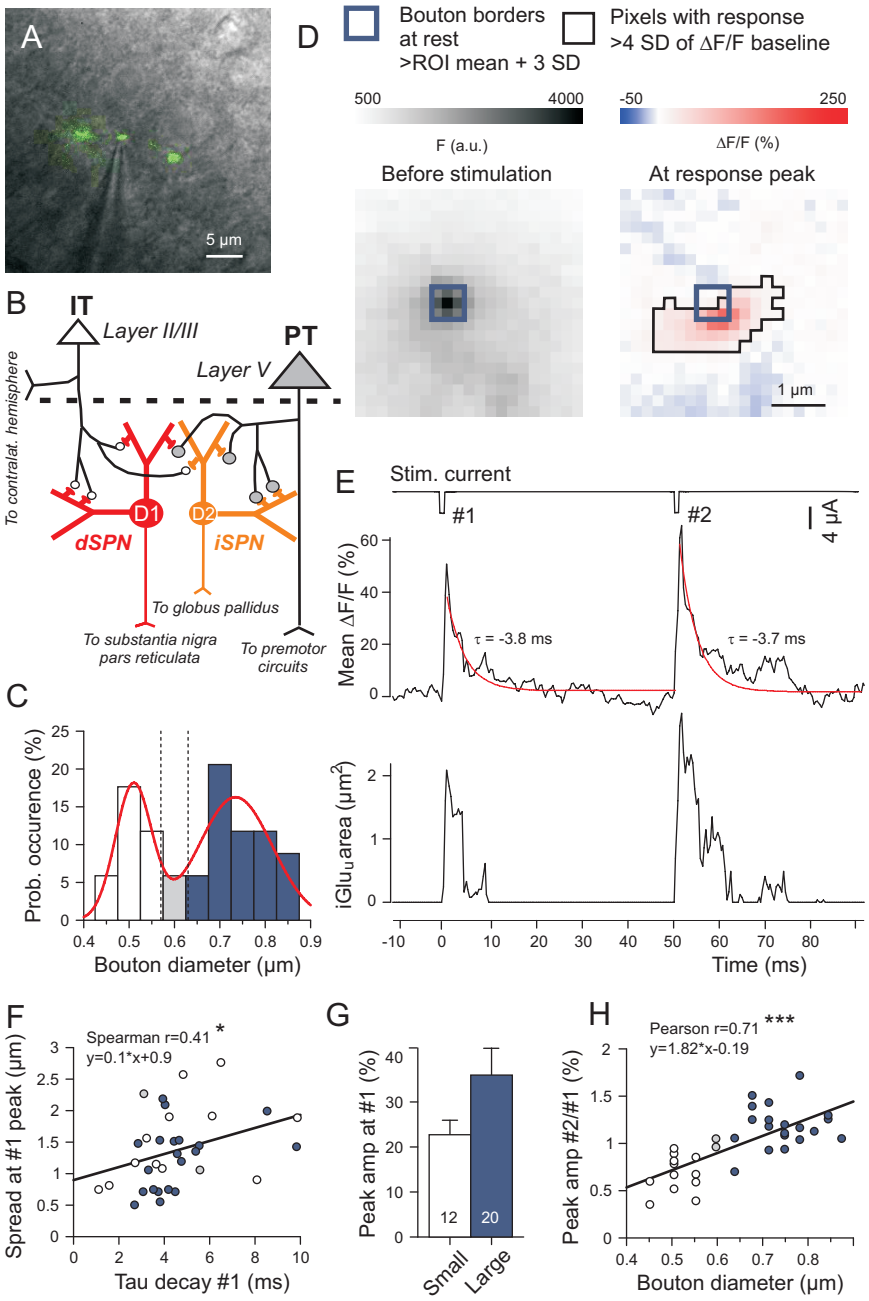

Fig. 1. Monitoring single synapse Glu transients in acute slices from adult mice after expression of the genetically encoded ultrafast Glu sensor iGlu$_u$ in corticostriatal neurons. (A) Resting iGlu$_u$ fluorescence merged to the respective 63x DIC image of a corticostriatal slice showing an axon with 3 adjacent varicosities and a stimulation pipette at the central bouton. (B) Simplified scheme of the corticostriatal circuitry (Reiner et al., 2010), illustrating the concept of preferential projection of pyramidal tract (PT) neurons to indirect pathway striatal projection neurons (iSPNs) and intratelencephalic (IT) neurons to direct pathway SPNs (dSPNs) and size-differences between the IT and PT terminals. Bimodal distribution of bouton diameters as determined by the supra-threshold resting fluorescence before stimulation. Boutons with diameter >= 0.63 µm were defined as "Large" and assumed to be issued by PT axons. (D) Example of a type PT bouton with the respective iGlu$_u$ fluorescence at rest (left) and at the peak of an AP-mediated iGlu$_u$ response (right). (E) iGlu$_u$ responses recorded from the bouton shown in (A, D). Experiment in 2 mM Ca^{2+} and 1 mM Mg^{2+}. Simultaneous recording of stimulation current (upper trace), mean supra-threshold pixel intensity (middle trace) and the area of supra-threshold pixels (bottom trace). A monoexponential function is fitted to the decay of the 1st (#1) iGlu$_u$ transient with the respective time constants shown next to the fitting curves. (F) Positive correlation between the "Spread" at the time of peak and TauD after stimulus #1. (G) Peak amplitudes of responses to stimulus #1. There is no difference between small and large terminals. (H) Significant correlation between the PPR of peak amplitudes and bouton diameter for single or #1 stimuli.

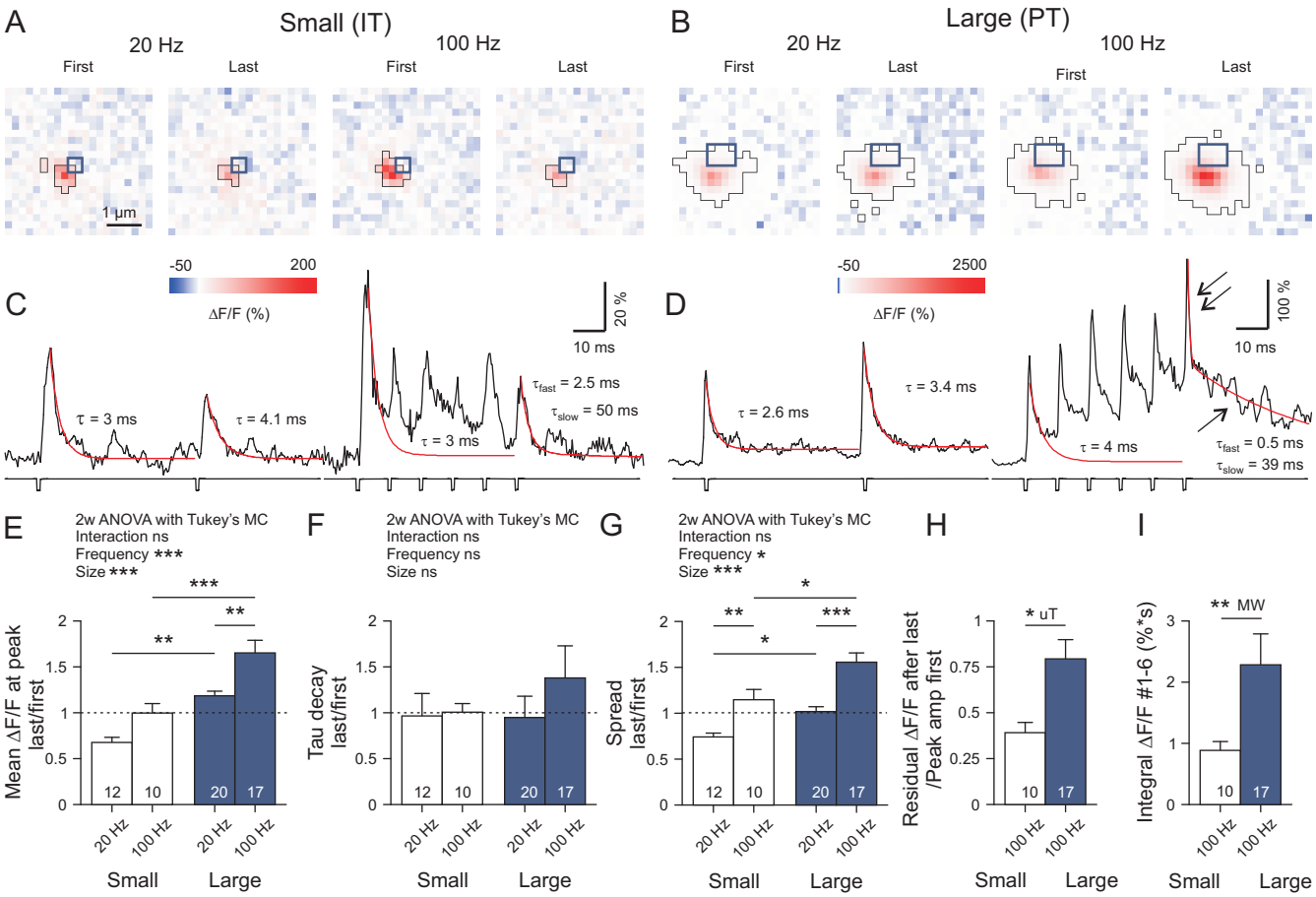

Fig. 2. Contrasting dynamics of Glu release from small and large corticostriatal terminals. (A-D) Specimen records of AP-mediated $iGlu_u$ signals at 20 and 100 Hz, as derived from small and large boutons. All $iGlu_u$ transients were elicited in an AP-dependent manner in 2 mM Ca^{2+}. Experimental conditions as in Fig. 1. (E-I) Quantification of results. The large terminals produced a significant build-up of residual $iGlu_u$ fluorescence (single arrow) that added to the fast stimulus-locked transients (double arrow). Note that the time integral of all supra-threshold pixel intensities generated by a 6-pulse train at 100 Hz during a sampling period of 70 ms was much bigger in large boutons (I).

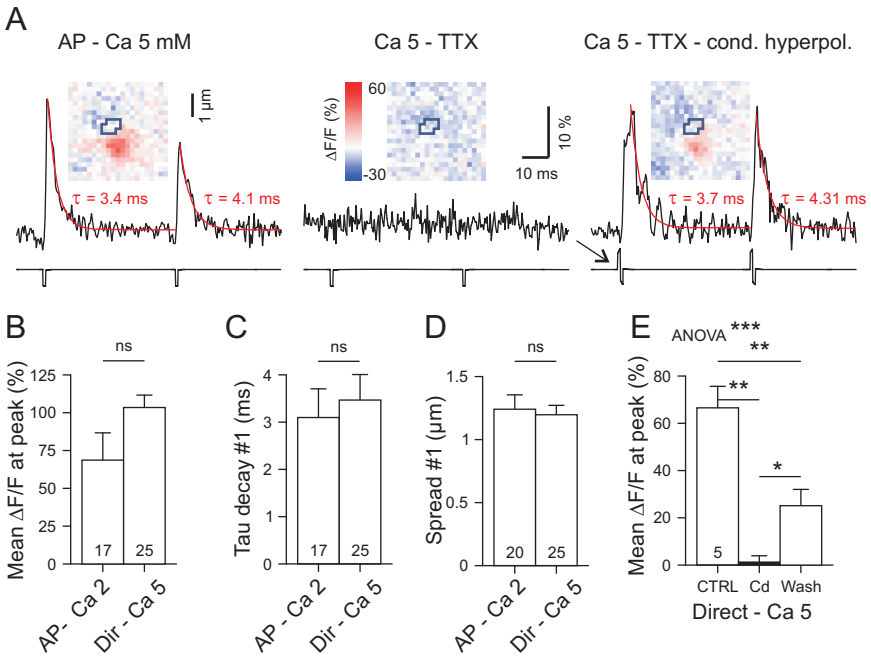

Fig. 3. Responses to directly induced test pulses by-passing the AP mechanism in WT boutons of type P. (A) Experiment in elevated $[Ca^{2+}]_{ec}$. Left: Response to electrical stimulation in the absence of TTX elicited by a short (1 ms) depolarizing pulse. In 5 mM Ca^{2+} the AP-mediated response exhibits paired pulse depression. Middle: same condition but in the presence of TTX. Note complete block of Glu release. Right: Response in 5 mM Ca^{2+} and TTX, but elicited with the 1 ms depolarizing pulse preceded by a short hyperpolarizing pulse, to recruit additional Ca^{2+} channels. (B) Stimulus intensity for direct activation of Glu release was adjusted such that the amplitudes of $iGlu_u$ signals matched the amplitudes observed with the last (#6) stimulus in a 100 Hz train under physiological conditions (2 mM Ca^{2+} and intact AP generation). (C, D) Lack of differences between physiological and test pulse-induced responses. (E) The directly induced responses were completely blocked by Cd^{2+} (500 µM).

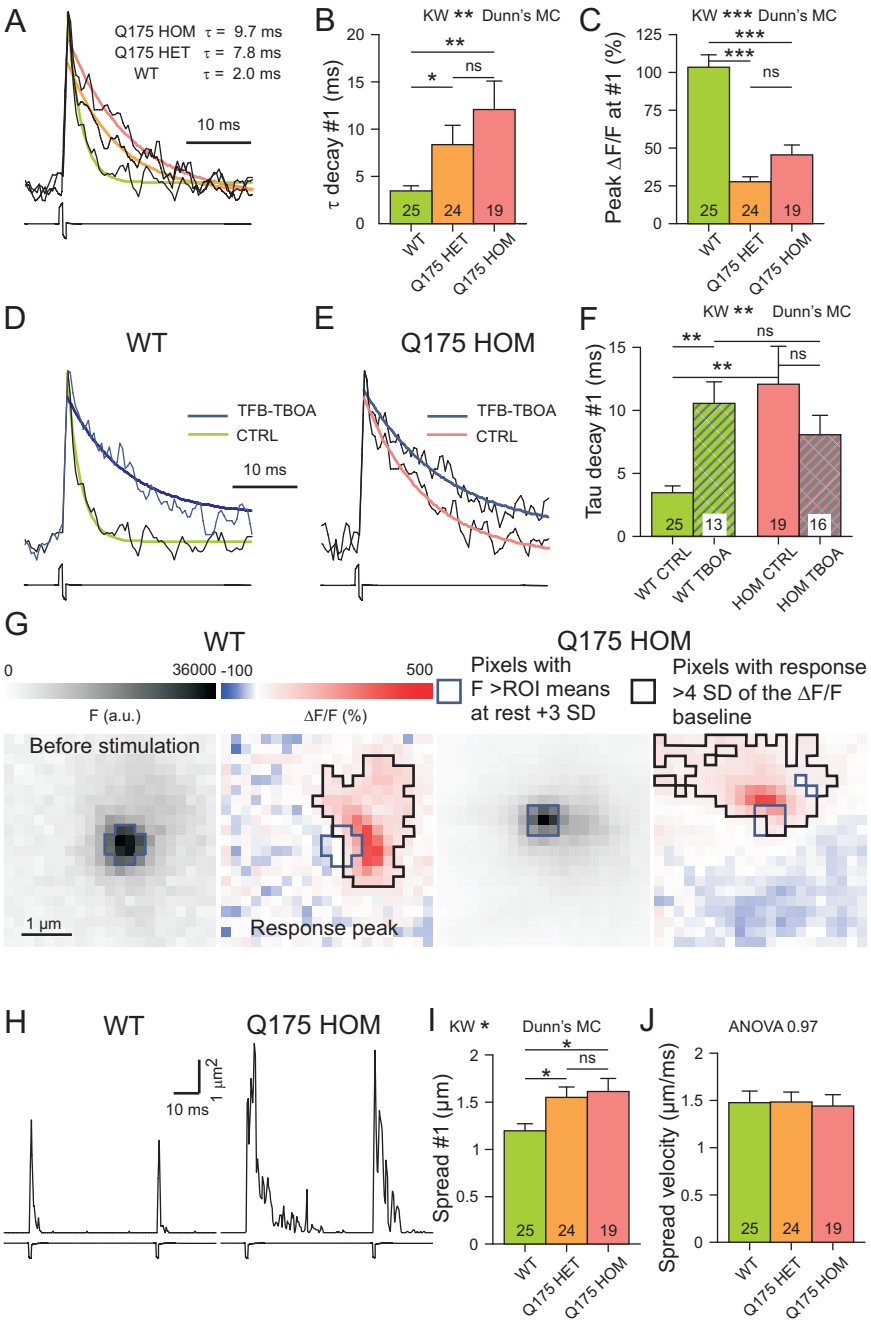

Fig. 4. HD-related differences in the clearance of synaptically released Glu. (A) Specimen records of iGlu$_u$ responses to direct activation of a P-type varicosity in the presence of TTX. Fitting a monoexponential function to the decay of the iGlu$_u$ transient of Q175 WT (green), HET (orange) and HOM (red) revealed differences in the duration of the Glu transient. The amplitudes were normalized to the same peak value. (B, C) Quantification of the results from WT (green), HET (orange) and HOM (red). (D-F) Incubation of WT slices in 100 nM of TFB-TBOA simulated the depression of Glu clearance observed in HOM. (G, H) Specimen images and traces, showing the "Spread" in WT and HD mice. (I, J) Quantification of results from analysis of the iGlu$_u$ signals in WT and HD mice. The "Spread" in (I) refers to the diameter of the supra-threshold pixel area approximated as a circle in the X-Y plane.

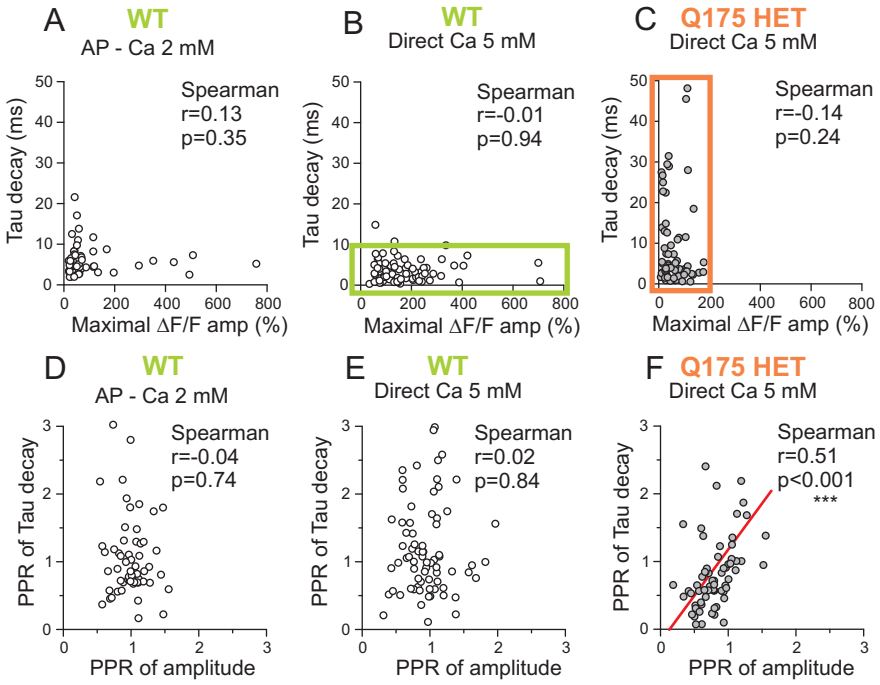

Fig. 5. HD-related differences in Glu release and uptake. (A-C) Correlograms of TauD and maximal ΔF/F amplitudes in WT (A) and in Q175 HET (B, C). To emphasize the HD-related differences in the range of obtained values, the data points were boxed green in WT and red in Q175 HET. (D-F) Correlograms of TauD and peak amplitudes of ΔF/F. To eliminate inter-synapse variability, #2 responses were normalized to #1 responses. The inter-trial variability of responses elicited at a repetition frequency of 0.1 Hz was used to test for a positive correlation between TauD and peak amplitudes of ΔF/F. Note positive correlation in HET (F) but not WT (D, E). Data from HET: 11 animals, 23 synapses, 3 trials per synapse.

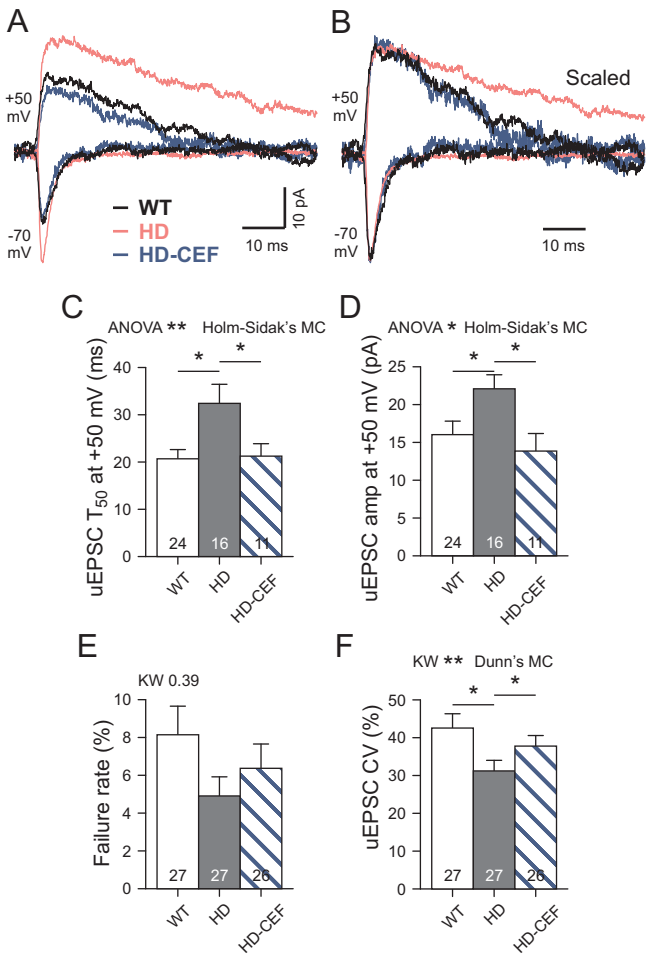

Fig. 6. HD-related prolongation of the NMDAR component in uEPSCs elicited by optical stimulation of single corticostriatal afferents visualized by EYFP fluorescence after the expression of CaMKIIa.hChR2(E123T/T159C)-EYFP.hGH. *(A)* Specimen traces as recorded at two different holding potentials in the presence of bicuculline methiodide (25 μM). *(B)* Same traces as *(A)* but aligned to peak. See prolonged decay in comparison with records at -70 mV. This difference was abolished by APV (not illustrated), and more pronounced in Q175 HOM (red traces). Treatment with CEF abolished the uEPSC prologation at +50 mV (blue traces). *(C-F)* Quantification of results. Note significantly larger T50 values of the NMDAR-mediated response at +50 mV and recovery after CEF treatment *(C)*.

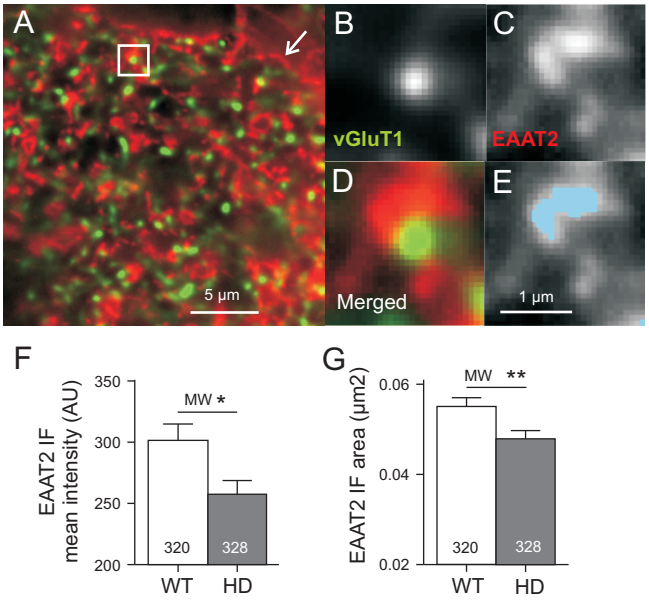

Fig. 7. Lower than in WT perisynaptic EAAT2 immunofluorescence in Q175 HOM. (A) Merged image of a view-field in the dorsal striatum showing the vGluT1 IF of corticostriatal synaptic terminals (green) and EAAT2 IF clusters (red) in the immediate vicinity of vGLUT+ terminals and in contact with a blood vessel (arrow). (B-C) Enlarged images of the (ROI) boxed in (A), with separate (B, C) and merged (D) channels. (E) Pixels with supra-threshold EAAT2 IF (light blue). (F, G) Mean intensity and area of supra-threshold pixels in the dorsal striatum of WT and Q175 HOM. Numbers refer to the number of ROIs, each comprising one vGluT1+ varicosity. Data from 4 WT and 4 Q175 HOM.

iGlu$_u$ signals at IT vs. PT terminals	Varicosities type "Small" (IT)				Varicosities type "Large" (PT)				Statistics
	Mean	SE	N-T	N-A	Mean	SE	N-T	N-A	Pvalues/Test
Diameter, from F at rest (µm)	0.51	0.01	12	6	0.78	0.01	25	3	*0.0001/MW*
Maximal amp* #1** (%)	63.50	17.53	12	6	100.22	33.13	20	10	*0.5700/MW*
Peak amp all supraThr *** #1 (%)	22.72	3.22	12	6	35.97	6.02	20	10	*0.1300/MW*
TauD all supraThr #1 (ms)	4.65	0.75	12	6	4.56	0.39	20	10	*0.9500/MW*
Spread all supraThr #1 (µm)	1.54	0.19	12	6	1.24	0.11	20	10	*0.1600/ uT*
PPR peak amp all supraThr (#2/ #1)	0.68	0.06	12	6	1.18	0.05	20	10	*0.0001/ uT*
Maximal amp after #6, 100 Hz (%)	44.35	11.19	10	6	220.79	105.83	17	9	*0.0020/MW*
Peak amp amp all supraThr after #6, 100 Hz (%)	24.96	3.56	10	6	68.67	18.01	17	9	*0.0010/MW*
Residual ΔF/F after #6, 100 Hz (%)	7.47	1.78	10	6	28.13	6.17	17	9	*0.0006/MW*
TauD residual ΔF/F after #6, 100 Hz (ms)	40.73	6.28	10	6	58.47	12.82	17	9	*0.8600/MW*
Spread all supraThr with residual ΔF/F after #6, 100 Hz (µm)	1.05	0.15	10	6	1.66	0.15	17	9	*0.0140/MW*

*Tab. 1. Comparison of iGlu$_u$ signals in varicosities type "Small" (presumably IT) and "Large" (presumably PT). * - pixel with highest ΔF/F. **# - stimulus number during repetitive activation. *** - supraThr - all supra-threshold pixels. N-T – number of terminals. N-A – number of animals. In bold: indicators with significant afferent-related difference. MW – Mann-Whitney test, uT – unpaired t test.*

Directly induced $iGlu_u$ transients at P-type terminals	WT				HET					HOM				
	Mean	**SE**	**N-T**	**N-A**	**Mean**	**SE**	**N-T**	**N-A**	**Δ (%WT)**	**Mean**	**SE**	**N-T**	**N-A**	**Δ (%WT)**
Max amp #1* (%)**	226.23	32.58	25	3	65.05	10.48	24	11	*-71*	155.07	33.52	19	3	*-31*
Peak amp all supraThr*** #1 (%)	103.44	8.21	25	3	27.72	3.29	24	11	*-73*	45.49	6.54	19	3	*-56*
TauD all supraThr #1 (ms)	3.47	0.54	25	3	8.36	2.04	24	11	*141*	12.08	3.01	19	3	*248*
Spread all supraThr #1 (µm)	1.20	0.07	25	3	1.55	0.11	24	11	*30*	1.61	0.14	19	3	*35*
PPR peak amp all supraThr (#2/ #1)	0.95	0.07	25	3	0.88	0.06	23	11	*ns*	0.82	0.13	19	3	*ns*
PPR TauD all supraThr (#2/ #1)	1.37	0.15	25	3	0.88	0.06	23	11	*-36*	0.73	0.12	19	3	*-46*

P values/Tests for comparison of genotypes	Tested genotype pairs		
	WT-HET	**WT-HOM**	**HET-HOM**
Max amp #1 (%)	*0.0001/MW*	*0.0200/MW*	*0.0100/MW*
Peak amp all supraThr #1 (%)	*0.0001/MW*	*0.0001/MW*	*0.0200/MW*
TauD all supraThr #1 (ms)	*0.0110/MW*	*0.0040/MW*	*0.4100/MW*
Spread all supraThr #1 (µm)	*0.0160/MW*	*0.0120/MW*	*0.7200/ uT*
PPR peak amp all supraThr (#2/ #1)	*0.1800/ uT*	*0.0900/MW*	*0.2900/MW*
PPR TauD all supraThr (#2/ #1)	*0.0400/MW*	*0.0030/ uT*	*0.3100/MW*

*Tab. 2. Comparison of WT and Q175 HET and HOM. * - pixel with highest ΔF/F. **# - stimulus number during repetitive activation. *** all supra-threshold pixels. N-T – number of terminals. N-A – number of animals. HET: 15-18 mo. HOM: 12-15 mo. Δ%WT – difference in comparison to WT in % mean WT value. In bold: indicators with significant genotype-related difference.*

Corticostriatal unitary EPSCs	WT				HOM					HOM+CEF					Pvalues/Test	
	Mean	SE	N		Mean	SE	N		Δ %WT	Mean	SE	N		Δ %WT	WT/HOM	HOM/ HOM+CEF
			C	A			C	A				C	A			
Amp NMDAR response* at +50 mV (pA)*	16.03	1.79	24	6	22.09	1.86	16	4	*38*	13.85	2.32	11	3	*ns*	*0.0300/uT*	*0.0099/ uT*
T50 of NMDAR response at +50 mV (ms)	20.68	1.95	24	6	32.41	4.03	16	4	*57*	21.25	2.63	11	3	*ns*	*0.0060/uT*	*0.0470/ uT*
Amp of AMPAR response* at -70 mV (pA)	29.07	2.82	27	6	38.71	2.54	27	5	*33*	30.05	3.03	26	5	*ns*	*0.0100/uT*	*0.0040/MW*
TauD AMPAR response at -70 mV (ms)	4.06	0.24	27	6	4.76	0.31	27	5	*ns*	4.05	0.29	26	5	*ns*	*0.1400/M*	*0.0600/MW*
CV of AMPAR response at -70 mV (pA)	42.55	3.78	27	6	31.21	2.80	27	5	*-27*	37.78	2.79	26	5	*ns*	*0.0040/M*	*0.0070/MW*
Failure rate AMPAR response at -70 mV	8.14	1.51	27	6	4.91	1.01	27	5	*ns*	6.37	1.29	26	5	*ns*	*0.1700/M*	*0.4700/MW*

*Tab. 3. Comparison uEPSCs in WT. Q175 HOM and Q175 HOM treated with ceftriaxone (CEF). *amplitude without failures. N – number of cells (C) or animals (A). ∆%WT – difference in % of mean WT value. In bold: Indicators with significant genotype- or treatment-related difference. MW – Mann-Whitney test, uT – unpaired t test.*